

UMAP-assisted K -means clustering of large-scale SARS-CoV-2 mutation datasets

Yuta Hozumi¹, Rui Wang¹, Changchuan Yin², and Guo-Wei Wei^{1,3,4*}

¹ Department of Mathematics,

Michigan State University, MI 48824, USA.

² Department of Mathematics, Statistics, and Computer Science,
University of Illinois at Chicago, Chicago, IL 60607, USA

³ Department of Electrical and Computer Engineering,
Michigan State University, MI 48824, USA.

⁴ Department of Biochemistry and Molecular Biology,
Michigan State University, MI 48824, USA.

Abstract

Coronavirus disease 2019 (COVID-19) caused by severe acute respiratory syndrome coronavirus 2 (SARS-CoV-2) has a worldwide devastating effect. The understanding of evolution and transmission of SARS-CoV-2 is of paramount importance for the COVID-19 control, combating, and prevention. Due to the rapid growth of both the number of SARS-CoV-2 genome sequences and the number of unique mutations, the phylogenetic analysis of SARS-CoV-2 genome isolates faces an emergent large-data challenge. We introduce a dimension-reduced k -means clustering strategy to tackle this challenge. We examine the performance and effectiveness of three dimension-reduction algorithms: principal component analysis (PCA), t -distributed stochastic neighbor embedding (t -SNE), and uniform manifold approximation and projection (UMAP). By using four benchmark datasets, we found that UMAP is the best-suited technique due to its stable, reliable, and efficient performance, its ability to improve clustering accuracy, especially for large Jaccard distanced-based datasets, and its superior clustering visualization. The UMAP-assisted k -means clustering enables us to shed light on increasingly large datasets from SARS-CoV-2 genome isolates.

Key words: PCA, t -SNE, UMAP, SARS-CoV-2, COVID-19

Contents

1	Introduction	1
2	Methods	2
2.1	Sequence and alignment	2
2.2	SNP position based features	3
2.3	Jaccard based representation	3
2.4	K -means clustering	3

*Corresponding author. E-mail: weig@msu.edu

2.5	Principal component analysis	4
2.6	t-SNE	4
2.7	UMAP	5
3	Validation	6
3.1	Validation data	7
3.2	Validation results	7
3.2.1	Coil 20	8
3.2.2	Facebook Network	9
3.2.3	MNIST	10
3.2.4	Jaccard distanced-based MNIST	12
3.3	Efficiency comparison	14
4	SARS-CoV-2 mutation clustering	14
4.1	World SARS-CoV-2 mutation clustering	14
4.2	United States SARS-CoV-2 mutation clustering	17
5	Discussion	18
6	Conclusion	20
7	Appendix	23

1 Introduction

Beginning in December 2019, coronavirus disease 2019 (COVID-19) caused by severe acute respiratory syndrome coronavirus 2 (SARS-CoV-2) has become one of the most deadly global pandemic in history. The COVID-19 infections in the US and other nations are still spiking. As of October 30, 2020, the World Health Organization (WHO) has reported 44,888,869 confirmed cases of COVID-19 and 1,178,145 confirmed deaths. The virus has spread to Africa, Americas, Eastern Mediterranean, Europe, South-East Asia and Western Pacific [1]. To prevent further damage to our livelihood, we must control its spread through testing, social distancing, tracking the spread, and developing effective vaccines, drugs, diagnostics, and treatments.

SARS-CoV-2 is a positive-sense single-strand RNA virus that belongs to the Nidovirales order, coronaviridae family and betacoronavirus genus [20]. To effectively track the virus, testing patients with suspected exposure to COVID-19 and sequencing the strand via PCR (polymerase chain reaction) are important. From sequencing, we can analyze patterns in mutation and predict transmission pathways. Without understanding such pathways, current efforts to find effective medicines and vaccines could become futile because mutations may change viral genome or lead to resistance. As of October 30, 2020, there are 89627 available sequences with 23763 unique single nucleotide polymorphisms (SNPs) with respect to the first SARS-CoV-2 sequent collected in December 2019 [35] according to our mutation tracker https://users.math.msu.edu/users/weig/SARS-CoV-2_Mutation_Tracker.html.

A popular method for understanding mutational trends is to perform phylogenetic analysis, where one clusters mutations to find evolution patterns and transmission pathways. Phylogenetic analysis has been done on the Nidovirales family [2,2,9,10,12,15] to understand genetic evolutionary pathways, protein level changes [6,12,30,31], large scale variants [30–32,34] and global trends [3,27,29]. Commonly used techniques for phylogenetic analysis include tree based methods [21] and K -means clustering. Both methods belong to unsupervised machine learning techniques, where ground truth is unavailable. These approaches provide valuable information for exploratory research. A main issue with phylogenetic tree analysis is that as the number of samples increase, its computation becomes unpractical, making it unsuitable for large genome datasets. In contrast, K -means scales well with sample size increase, but does not perform well when the sample size is too small. Jaccard distance is commonly used to compare genome sequences [36] because it offers a phylogenetic or topological difference between samples. However, the tradeoff to the Jaccard distance is that its feature dimension is the same as its number of samples, suggesting that for a large sample size, the number of features is also large. Since K -means clustering relies on computing the distance between the center of the cluster and each sample, having a large feature space can result in expensive computation, large memory requirement, and poor clustering performance. This become a significant problem as the number of SARS-CoV-2 genome isolates from patients has reached 150,000 at this point. There is a pressing need for efficient clustering methods for SARS-CoV-2 genome sequences.

One technique to address this challenge is to perform dimensional reduction on the K -means input dataset so that the task becomes manageable. Commonly used dimension reduction algorithms focus on two aspects: 1) the pairwise distance structure of all the data samples and 2) preservation of the local distances over the global distance. Techniques such as principal component analysis (PCA) [11], Sammon mapping [23], and multidimensional scaling (MDS) [8] aim to preserve the pairwise distance structure of the dataset. In contrast, the t-distributed stochastic neighbor embedding (t-SNE) [16,17], uniform manifold approximation and projection (UMAP) [4,18], Laplacian eigenmaps [5], and LargeVis [26] focus on the preservation of local distances. Among them, PCA, t-SNE, and UMAP are the most frequently used algorithms in the applications of cell biology, bioinformatics, and visualization [4].

PCA is a popular method used in exploratory studies, aiming to find the directions of the maximum variance in high-dimensional data and projecting them onto a new subspace to obtain low-dimensional

feature spaces while preserving most of the variance. The principal components of the new subspace can be interpreted as the directions of the maximum variance, which makes the new feature axes orthogonal to each other. Although PCA is able to cover the maximum variance among features, it may lose some information if one chooses an inappropriate number of principal components. As a linear algorithm, PCA performs poorly on the features with nonlinear relationship. Therefore, in order to present high-dimensional data on low dimensional and nonlinear manifold, some nonlinear dimensional reduction algorithms such as t-SNE and UMAP are employed. T-SNE is a nonlinear method that can preserve the local and global structures of data. There are two main steps in t-SNE. First, it finds a probability distribution of the high dimensional dataset, where similar data points are given higher probability. Second, it finds a similar probability distribution in the lower dimension space, and the difference between the two distributions is minimized. However, t-SNE computes pairwise conditional probabilities for each pair of samples and involves hyperparameters that are not always easy to tune, which makes it computationally complex. UMAP is a novel manifold learning technique that also captures a nonlinear structure, which is competitive with t-SNE for visualization quality and maintains more of the global structure with superior run-time performance [18]. UMAP is built upon the mathematical work of Belkin and Niyogi on Laplacian eigenmaps, aiming to address the importance of uniform data distributions on manifolds via Riemannian geometry and the metric realization of fuzzy simplicial sets by David Spivak [25]. Similar to t-SNE, UMAP can optimize the embedded low-dimensional representation with respect to fuzzy set cross-entropy loss function by using stochastic gradient descent. The embedding is found by finding a low-dimensional projection of the data that closely matches the fuzzy topological structure of the original space. The error between two topological spaces will be minimized by optimizing the spectral layout of data in a low dimensional space.

In this work, we explore efficient computational methods for the SARS-CoV-2 phylogenetic analysis of large volumn of SARS-CoV-2 genome sequences. Specifically, we are interested in developing a dimension-reduction assisted clustering method. To this end, we compare the effectiveness and accuracy of PCA, t-SNE and UMAP for dimension reduction in association with the K -means clustering. To quantitatively evaluate the performance, we recast supervised classification problems with labels into a K -means clustering problems so that the accuracy of K -means clustering can be evaluated. As a result, the accuracy and performance of PCA, t-SNE and UMAP-assisted K -means clustering can be compared. By choosing the different dimensional reduction ratios, we examine the performance of these methods in K -means settings on four standard datasets. We found that UMAP is the most efficient, robust, reliable, and accurate algorithm. Based on this finding, we applied the UMAP-assisted K -means technique to large scale SARS-CoV-2 datasets generated from a Jaccard distance representation and a SNP position-based representation to further analyze its effectiveness, both in terms of speed and scalability. Our results are compared with those in the literature [31] to shed new light on SARS-CoV-2 phylogenetics.

2 Methods

2.1 Sequence and alignment

The SARS-CoV-2 sequences were obtained from GISAID databank (www.gisaid.com). Only complete genome sequences with collection date, high coverage, and without 'NNNNNN' in the sequences were considered. Each sequence was aligned to the reference sequence [35] using a multiple sequence alignment (MSA) package Clustal Omega [24]. A total of 23763 complete SARS-CoV-2 sequences are analyzed in this work.

2.2 SNP position based features

Let N be the number of SNP profiles with respect to the SARS-CoV-2 reference genome sequence, and let M be the number of unique mutation sites. Denote V_i as the position based feature of the i th SNP profile.

$$V_i = [v_i^1, v_i^2, \dots, v_i^M], \quad i = 1, 2, \dots, N \quad (1)$$

is a $1 \times M$ vector. Here

$$v_i^j = \begin{cases} 1, & \text{mutation site} \\ 0, & \text{otherwise.} \end{cases} \quad (2)$$

We compile this into an $N \times M$ position based feature,

$$S(i, j) = v_i^j \quad (3)$$

where each row represents a sample. Note that $S(i, j)$ is a binary representation of the position and is sparse.

2.3 Jaccard based representation

The Jaccard distance measures the dissimilarity between two sets. It is widely used in the phylogenetic studies of SNP profiles. In this work, we utilize Jaccard distance to compare SNP profiles of SARS-CoV-2 genome isolates.

Let A and B be two sets. Consider the Jaccard index between A and B , denoted $J(A, B)$, as the cardinality of the intersection divided by the cardinality of the union

$$J(A, B) = \frac{|A \cap B|}{|A \cup B|} = \frac{|A \cap B|}{|A| + |B| - |A \cap B|}. \quad (4)$$

The Jaccard distance between the two sets is defined by subtracting the Jaccard index from 1:

$$d_J(A, B) = 1 - J(A, B) = \frac{|A \cup B| - |A \cap B|}{|A \cup B|} \quad (5)$$

We assume there are N SNP profiles or genome isolates that have been aligned to the reference SARS-CoV-2 genome. Let S_i , $i = 1, \dots, N$, be the set with the position of the mutation of the i th sample. The Jaccard distance between two sets S_i and S_j is given by $d_J(S_i, S_j)$. Taking the pairwise distance between all the samples, we can construct the Jaccard based representation, resulting in an $N \times N$ distance matrix D

$$D(i, j) = d_J(S_i, S_j) \quad (6)$$

This distance defines a metric over the collections of all finite sets [14].

2.4 K -means clustering

K -means clustering is one of the most popular unsupervised learning methods in machine learning, where it aims to cluster or partition a data $\{x_1, \dots, x_N\}$, $x_i \in \mathbb{R}^M$ into k clusters, $\{C_1, \dots, C_k\}$, $k \leq N$.

K -means clustering begins with selecting k points as k cluster centers, or centroids. Then, each point in the dataset is assigned to the nearest centroid. The centroids are then updated by minimizing the within-cluster sum of squares (WCSS), which is defined as

$$\sum_{i=1}^k \sum_{x_i \in C_k} \|x_i - \mu_k\|_2^2. \quad (7)$$

Here, $\|\cdot\|_2$ denotes the l_2 norm and μ_k is the average of the data point in cluster k

$$\mu_k = \frac{1}{|C_k|} \sum_{x_i \in C_k} x_i. \quad (8)$$

This method, however, only finds the optimal centroid, given a fixed number of clusters k . In applications, we are interested in finding the optimal number of clusters as well. In order to obtain the best k clusters, elbow method was used. The optimal number of clusters can be determined via the elbow method by plotting the WCSS against the number of clusters, and choosing the inflection point position as the optimal number of clusters.

2.5 Principal component analysis

Principal component analysis (PCA) is one the most commonly used dimensional reduction techniques for the exploratory analysis of high-dimensional data [11]. Unlike other methods, there is no need for any assumptions in the data. Therefore, it is a useful method for new data, such as SARS-CoV-2 SNPs data. PCA is conducted by obtaining one component or vector at a time. The first component, termed the principal component, is the direction that maximizes the variance. The subsequent components are orthogonal to earlier ones.

Let $\{x_i\}_{i=1}^N$ be the input dataset, with N being the number of samples or data points. For each x_i , let $x_i \in \mathbb{R}^M$, where M is the number of features or data dimension. Then, we can cast the data as a matrix $X \in \mathbb{R}^{N \times M}$. PCA seeks to find a linear combination of the columns of X with maximum variance.

$$\sum_{j=1}^n a_j x_j = Xa, \quad (9)$$

where a_1, a_2, \dots, a_n are constants. The variance of this linear combination is defined as

$$\text{var}(Xa) = a^T S a, \quad (10)$$

where S is the covariance matrix for the dataset. Note that we compute the eigenvalue of the covariance matrix. The maximum variance can be computed iteratively using Rayleigh's quotient

$$a_{(1)} = \arg \max_a \frac{a^T X^T X a}{a^T a}. \quad (11)$$

The subsequent components can be computed by maximizing the variance of

$$\hat{X}_k = X - \sum_{j=1}^{k-1} X a_j a_j^T \quad (12)$$

where k represents the k th principal component. Here, $k - 1$ principal components are subtracted from the original matrix X . Therefore, the complexity of the method scales linearly with the number of components one seeks to find. In applications, we hope that the first few components give rise to a good PCA representation of the original data matrix X .

2.6 t-SNE

The t-distributed stochastic neighbor embedding (t-SNE) is a nonlinear dimensional reduction algorithm that is well suited for reducing high dimensional data into the two- or three-dimensional space. There are two main stages in t-SNE. First, it constructs a probability distribution over pairs of data such that a pair

of near data points is assigned with a high probability, while a pair of farther away points is given a low probability. Second, t-SNE defines a probability distribution in the embedded space that is similar to that in the original high-dimensional space, and aims to minimize the Kullback-Leibler (KL) divergence between them [16].

Let $\{x_1, x_2, \dots, x_N | x_i \in \mathbb{R}^M\}$ be a high dimensional input dataset. Our goal is to find an optimal low dimensional representation $\{y_1, \dots, y_N | y_i \in \mathbb{R}^k\}$, such that $k \ll M$. The first step in t-SNE is to compute the pairwise distribution between x_i and x_j , defined as p_{ij} . However, we find the conditional probability of x_j , given x_i :

$$p_{j|i} = \frac{\exp(-\|x_i - x_j\|^2 / 2\sigma_i^2)}{\sum_{m \neq i} \exp(-\|x_i - x_m\|^2 / 2\sigma_i^2)}, \quad i \neq j, \quad (13)$$

setting $p_{i|i} = 0$, and the denominator normalizes the probability. Here, σ_i is the predefined hyperparameter called perplexity. A smaller σ_i is used for a denser dataset. Notice that this conditional probability is symmetric when the perplexity is fixed, i.e. $p_{i|j} = p_{j|i}$. Then, define the pairwise probability as

$$p_{ij} = \frac{p_{j|i} + p_{i|j}}{2N}. \quad (14)$$

In the second step, we learn a k -dimensional embedding $\{y_1, \dots, y_N | y_i \in \mathbb{R}^k\}$. To this end, t-SNE calculates a similar probability distribution q_{ij} defined as

$$q_{ij} = \frac{\frac{1}{1 + \|y_i - y_j\|^2}}{\sum_m \sum_{l \neq m} \frac{1}{1 + \|y_m - y_l\|^2}}, \quad i \neq j \quad (15)$$

and setting $q_{ii} = 0$. Finally, the low dimensional embedding $\{y_1, \dots, y_N | y_i \in \mathbb{R}^k\}$ is found by minimizing the KL-divergence via a standard gradient descent method

$$\text{KL}(P|Q) = \sum_{i,j} p_{ij} \log \frac{p_{ij}}{q_{ij}}, \quad (16)$$

where P and Q are the distributions for p_{ij} and q_{ij} , respectively. Note that the probability distributions in Eqs. (13) and (15) can be replaced by using many other delta sequence kernel of positive type [33].

2.7 UMAP

Uniform manifold approximation and projection (UMAP) is a nonlinear dimensional reduction method, utilizing three assumptions: the data is uniformly distributed on Riemannian manifold, Riemannian metric is locally constant, and the manifold is locally connected. Unlike t-SNE which utilizes probabilistic model, UMAP is a graph-based algorithm. Its essentially idea is to create a predefined k -dimensional weighted UMAP graph representation of each of the original high-dimensional data point such that the edge-wise cross-entropy between the weighted graph and the original data is minimized. Finally, the k -dimensional eigenvectors of the UMAP graph are used to represent each of the original data point. In this section, a computational view of UMAP is presented. For a more theoretical account, the reader is referred to Ref. [18].

Similar to t-SNE, UMAP considers the input data $X = \{x_1, x_2, \dots, x_N\}$, $x_i \in \mathbb{R}^M$ and look for an optimal low dimensional representation $\{y_1, \dots, y_N | y_i \in \mathbb{R}^k\}$, such that $k < M$. The first stage is the construction of weighted k -neighbor graphs. Let define a metric $d : X \times X \rightarrow \mathbb{R}^+$. Let $k \ll M$ be a hyperparameter, and compute the k -nearest neighbors of each x_i under a given metric d . For each x_i , let

$$\rho_i = \min\{d(x_i, x_j) | 1 \leq j \leq k, d(x_i, x_j) > 0\} \quad (17)$$

where σ_i is defined via

$$\sum_{j=1}^k \exp\left(\frac{-\max(0, d(x_i, x_j) - \rho_i)}{\sigma_i}\right) = \log_2 k. \quad (18)$$

One chooses ρ_i to ensure at least one data point is connected to x_i and having edge weight of 1, and set σ_i as a length scale parameter. One defines a weighted directed graph $\bar{G} = (V, E, \omega)$, where V is the set of vertices (in this case, the data X), E is the set of edges $E = \{(x_i, x_j) | 1 \leq h \leq k, 1 \leq i \leq N\}$, and ω is the weight for edges

$$\omega(x_i, x_j) = \exp\left(\frac{-\max(0, d(x_i, x_j) - \rho_i)}{\sigma_i}\right). \quad (19)$$

UMAP tries to define an undirected weighted graph G from directed graph \bar{G} via symmetrization. Let A be the adjacency matrix of the graph \bar{G} . A symmetric matrix can be obtained

$$B = A + A^T - A \otimes A^T, \quad (20)$$

where T is the transpose and \otimes denotes the Hadamard product. Then, the undirected weighted Laplacian G (the UMAP graph) is defined by its adjacency matrix B .

In its realization, UMAP evolves an equivalent weighted graph H with a set of points $\{y_i\}_{i=1, \dots, N}$, utilizing attractive and repulsive forces. The attractive and repulsive forces at coordinate y_i and y_j are given by

$$\frac{-2ab\|y_i - y_j\|_2^{2(b-1)}}{1 + \|y_i - y_j\|_2^2} w(x_i, x_j)(y_i - y_j), \quad \text{and} \quad (21)$$

$$\frac{2b}{(\epsilon + \|y_i - y_j\|_2^2)(1 + a\|y_i - y_j\|_2^{2b})} (1 - w(x_i, x_j))(y_i - y_j) \quad (22)$$

where a, b are hyperparameters, and ϵ is taken to be a small value such that the denominator does not become 0. The goal is to find the optimal low-dimensional coordinates $\{y_i\}_{i=1}^N, y_i \in \mathbb{R}^k$, that minimizes the edge-wise cross entropy with the original data at each point. The evolution of the UMAP graph Laplacian G can be regarded as a discrete approximation of the Laplace-Beltrami operator on a manifold defined by the data [7]. Implementation and further detail of UMAP can be found in Ref. [18].

UMAP may not work well if the data points is non-uniform. If part of the data points have k important neighbors while other part of the data points have $k' \gg k$ important neighbors, the k -dimensional UMAP will not work efficiently. Currently, there is no algorithm to automatically determine the critic minimal k_{\min} for a given dataset. Additionally, weights $w(x_i, x_j)$ and force terms can be replaced by other functions that are easier to evaluate [33]. The metric d can be selected as Euclidean distance, Manhattan distance, Minkowski distance, and Chebyshev distance, depending on applications.

3 Validation

K -means clustering is one of the unsupervised learning algorithms, suggesting that neither the accuracy nor the root-mean-square error can be calculated to evaluate the performance of the K -means clustering explicitly. Additionally, K -means clustering can be problematic for high-dimensional large datasets. Dimension-reduced K -means clustering is an efficient approach. To evaluate its accuracy and performance, we convert supervised classification problems with known salutations into dimension-reduced K -means clustering problems. In doing so, we apply the K -means clustering to the classification dataset by setting the number of clusters equals to the number of the real categories. Next, in each cluster, we will take the data with the dominant label as the test for all samples and then calculate the K -means clustering accuracy for the whole dataset.

3.1 Validation data

In this work, we will consider the following classification datasets to test the performance of the clustering methods: Coil 20, Facebook large page-page network, MNIST, and Jaccard distanced-based MNIST.

- **Coil 20:** Coil 20 [19] is a dataset with 1440 gray scale images, consisting of 20 different objects, each with 72 orientation. Each image is of size 128×128 , which was treated as a 16384 dimensional vector for dimensional reduction
- **Facebook Network:** Facebook large page-page network [22] is a page-page webgraph of verified Facebook sites. Each node represents a facebook page, and the links are the mutual links between sites. This is a binary dataset with 22,470 nodes; hence the sample size and feature size are both 22,470. Jaccard distance was computed between each nodes for the feature space.
- **MNIST:** MNIST [13] is a hand written digit dataset. Each image is a grey scale of size 28×28 , which was treated as a 784 dimensional vector for the feature space, each with a integer value in $[0, 255]$. Standard normalization was used before performing dimensional reduction. There are 70,000 sample, with 10 different labels.
- **Jaccard distanced-based MNIST:** The above dataset was converted to a Jaccard distance-based dataset. This is to simulate position based mutational dataset, where 1 indicates a mutation in a particular position. Jaccard distance was used to construct the feature space, hence for each sample, the feature size is 70,000. This dataset can be viewed as an additional validation on our Jaccard distance representation.

3.2 Validation results

In the present work, we implement three popular dimensional reduction methods, PCA, UMAP, and t-SNE, for the dimension reduction and compare their performance in K -means clustering. For a uniform comparison, we reduce the dimensions of the samples by a set of ratios. The minimum between the number of features and the number of samples was taken as base of the reduction. For the Coil 20 dataset, since the numbers of samples and features were 1440 and 16384, respectively, dimension-reductions were based on 1440. For the Facebook Network, since the numbers of samples and features were both 22,470, dimension-reductions were based on 22,470. For the MNIST dataset, since the numbers of samples and features were respectively 70,000 and 784, dimension-reductions were based on 784. Finally, for the Jaccard distanced-based MNIST dataset, since the numbers of samples and features were both 70,000, dimension-reductions were based on 70,000. Note that for the Jaccard distanced-based MNIST data, more aggressive ratios were used because the original feature size is huge, i.e., 70,000. The standard ratios of 2, 4, and 8, etc do not sufficiently reduce the dimension for effective K -means computation. For the purpose of visualization, two-dimensional reduction algorithms are applied to each reduction scheme. In order to validate PCA, UMAP, and t-SNE assisted K -means clustering, we observed their performance using labeled datasets. K -nearest neighbors (K -NN) was used to find the baseline of the reduction, which reveals how much information can be preserved in the feature after applying a dimensional reduction algorithm. For k -NN, 10 fold cross-validation was performed.

Notably, K -means clustering is an unsupervised learning algorithm, which does not have labels to evaluate the clustering performance explicitly. However, we can assess the K -means clustering accuracy via labeled datasets that has ground truth. In doing so, we choose the number of K as the original number of classes. Then, we can compared the k -means clustering results with the ground truth. Therefore, the accuracy can reveal the performance of the proposed dimension-reduction-assisted (k -means) clustering method. For the classification problem, we assume the training set is $\{(\mathbf{x}_i, y_i) | \mathbf{x}_i \in \mathbb{R}^m, y_i \in \mathbb{Z}\}_{i=1}^n$ with the $|\{y_i\}_{i=1}^n| = k$. Here n , m , and k represent the number of samples, the number of features $\{\mathbf{x}_i\}$, and the

number of labels $\{y_i\}$, respectively. We set the number of clusters equals to the number of labels k . After applying the K -means clustering algorithm, we get k different clusters $\{c_j\}_{j=1}^k$. In each cluster, we define the predictor of the K -means clustering in the cluster c_j to be :

$$\hat{y}(c_j) = \max\{F_j(y_1), \dots, F_j(y_k)\}, \quad (23)$$

where $F_j(y_i), \dots, F_j(y_k)$ are the appearance frequencies of each label in the cluster c_j . Then the clustering accuracy can be defined as:

$$\text{Accuracy} = \frac{\sum_i 1_{\{y_i = \hat{y}_i\}}}{n}, \quad (24)$$

where $\{\hat{y}_i\}$ are predicted labels. Moreover, other evaluation metrics such as precision, recall, and receiver operating characteristic (ROC) can also be defined accordingly.

3.2.1 Coil 20



Figure 1: Comparison of different dimensional reduction algorithms on Coil 20 dataset. Total 20 different labels are in the Coil 20 dataset, and we use the ground truth label to color each data points. (a) Feature size is reduced to dimension 2 by PCA. (b) Feature size is reduced to dimension 2 by t-SNE. (c) Feature size is reduced to dimension 2 by UMAP.

Figure 1 shows the performance of PCA-assisted, UMAP-assisted and t-SNE-assisted clustering of the Coil 20 dataset. For each case, the dataset were reduced to dimension 2 using default parameters, and the plots were colored with the ground truth of the Coil 20 dataset. It can be seen that PCA does not present good clustering, whereas UMAP and t-SNE show very good clusters.

Table 1: Accuracy of k -NN of the Coil 20 dataset without applying any reduction algorithms, as well as the accuracy of k -NN assisted by PCA, UMAP and t-SNE with different dimensional reduction ratio. The sample size, feature size, and the number of labels of the Coil 20 dataset are 1440, 16384, and 20, respectively.

Dataset	k -NN accuracy w/o reduction	Reduced dimension	PCA accuracy	UMAP accuracy	t-SNE accuracy
Coil 20 (1440,16384,20)	0.956	720 (1/2)	0.955	0.668	0.850
		360 (1/4)	0.957	0.861	0.889
		180 (1/8)	0.973	0.867	0.881
		90 (1/16)	0.977	0.860	0.885
		45 (1/32)	0.980	0.861	0.875
		22 (1/64)	0.985	0.868	0.743
		14 (1/100)	0.730	0.851	0.878
		7 (1/200)	0.985	0.870	0.845
		3	0.850	0.863	0.959
		2	0.730	0.853	0.948

Table 1 shows the accuracy of k -NN clustering of the Coil 20 dataset assisted by PCA, t-SNE, and UMAP with different dimensional reduction radio. The Coil 20 dataset has 1,440 samples, 16,384 features, and 20 different labels. For PCA, the sklearn implementation on python was used with standard parameters. Note that for all methods, dimensions were reduced to 3 and 2 for a comparison. For t-SNE, Multicore-TSNE [28]

was used because it offers up to 8 core processor, which is not available in the sklearn implementation, and it is the fastest performing t-SNE algorithm. For UMAP, we used standard parameters [18]. It can be seen that when we reduce the dimension to 3, t-SNE performs best. Moreover, when the dimensional reduction ratio is 1/100, PCA and UMAP also perform well. Notably, the k -NN accuracy for the data without applying any dimensional reduction algorithm is 0.956, indicating that UMAP does not provide the best clustering performance on the Coil 20 dataset. However, PCA and t-SNE will preserve the information of the original data with a dimensional reduction ratio larger than 1/100, and t-SNE even performs better for dimensional three on the Coil 20 dataset.

Table 2: Accuracy of K -means clustering of the Coil 20 dataset without applying any reduction algorithms, as well as the accuracy of K -means assisted by PCA, UMAP and t-SNE with different dimensional reduction ratio. The sample size, feature size, and the number of labels of the Coil 20 dataset are 1440, 16384, and 20, respectively.

Dataset	K -means accuracy w/o reduction	Reduced dimension	PCA accuracy	UMAP accuracy	t-SNE accuracy
Coil 20 (1440,16384,20)	0.626	720 (1/2)	0.64	0.301	0.798
		360 (1/4)	0.678	0.800	0.718
		180 (1/8)	0.633	0.822	0.648
		90 (1/16)	0.642	0.799	0.681
		45 (1/32)	0.666	0.800	0.615
		22 (1/64)	0.673	0.819	0.151
		14 (1/100)	0.631	0.817	0.154
		7 (1/200)	0.591	0.819	0.360
		3	0.561	0.800	0.780
2	0.537	0.801	0.828		

Table 2 describes the accuracy of K -means clustering of Coil 20 assisted by PCA, UMAP, and t-SNE with different dimensional reduction ratio. For consistency, we use the same set of standard parameters as k -NN. For the Coil 20 dataset, the accuracy of K -means clustering assisted by UMAP has the best performance. When the reduced dimension is 2048 (ratio 1/8), UMAP will result in a relatively high K -means accuracy (0.822). Moreover, although PCA performs best on k -NN accuracy, it performs poorly on the K -means accuracy, indicating that PCA is not a suitable dimensional reduction algorithm on the Coil 20 dataset. Furthermore, the highest accuracy of K -means clustering is 0.828, which is calculated from the t-SNE-assisted algorithm. However, the t-SNE-assisted accuracy under different reduction ratio changes dramatically. When the ratio is 1/64, the t-SNE-assisted accuracy is only 0.151, indicating that t-SNE is sensitive to the hyper-parameters settings. In contrast, the performance of UMAP is highly stable under all dimension-reduction ratios.

Note that dimension-reduced k -means clustering methods outperform the original k -means clustering. Therefore, the proposed dimension-reduced k -means clustering methods not only improve the k -means clustering efficiency, but also achieve better accuracy.

3.2.2 Facebook Network

Figure 2 shows the visualization performance of PCA-assisted, UMAP-assisted, and t-SNE-assisted clustering of the Facebook Network. For each case, the dataset was reduced to dimension 2 using default parameters, and the plots were colored with the ground truth of the Facebook Network. Figure 2 shows that the PCA-based data is located distributively, while the t-SNE- and UMAP-based data show clusters.

Table 3 shows the accuracy of k -NN clustering of the Facebook Network assisted by PCA, t-SNE, and UMAP with different dimensional reduction ratio. The Facebook Network dataset has 22,470 samples with 4 different labels, and the feature size of the Facebook Network is also 22,470. For each algorithm, we use the same settings as the Coil 20 dataset. Without applying any dimensional reduction method, The Facebook

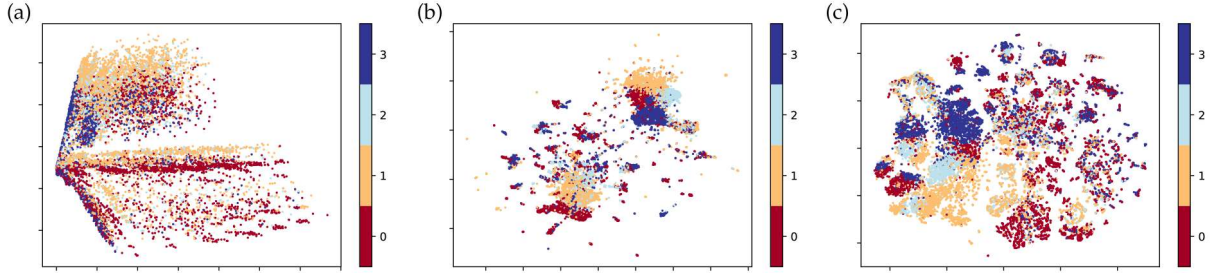


Figure 2: Comparison of different dimensional reduction algorithms on the Facebook Network dataset. Total 4 different labels are in the Facebook Network dataset, and we use the ground truth label to color each data points. (a) Feature size is reduced to dimension 2 by PCA. (b) Feature size is reduced to dimension 2 by t-SNE. (c) Feature size is reduced to dimension 2 by UMAP.

Network has 0.755 k -NN accuracy. The reduced feature from PCA has the best k -NN performance when the reduction ratio is 1/2. UMAP has a better performance compared to PCA and t-SNE when the reduction ratio is smaller than 1/16.

Table 3: Accuracy of k -NN of the Facebook Network without applying any reduction algorithms, as well as the accuracy of k -NN assisted by PCA, UMAP and t-SNE with different dimensional reduction ratio. The sample size, feature size, and the number of labels of the Facebook Network are 22470, 22470, and 4, respectively.

Dataset	k -NN accuracy w/o reduction	Reduced dimension	PCA accuracy	UMAP accuracy	t-SNE accuracy
Facebook Network (22470, 22470, 4)	0.755	11235 (1/2)	0.756	0.360	0.307
		5617 (1/4)	0.755	0.669	0.316
		2808 (1/8)	0.754	0.754	0.355
		1404 (1/16)	0.751	0.816	0.707
		702 (1/32)	0.751	0.814	0.669
		351 (1/64)	0.746	0.815	0.690
		224 (1/100)	0.733	0.814	0.676
		112 (1/200)	0.721	0.819	0.633
		44 (1/500)	0.714	0.816	0.709
		22 (1/1000)	0.690	0.815	0.643
		3	0.552	0.801	0.741
		2	0.501	0.786	0.732

Table 4 describes the accuracy of K -means clustering of the Facebook Network assisted by PCA, UMAP and t-SNE with different dimensional reduction ratio. PCA, UMAP, and t-SNE all have very poor performance, which may be caused by the smaller number of labels. The highest accuracy 0.427 is observed in the t-SNE-assistant algorithm with dimension 2.

Similar to the last case, UMAP-based and t-SNE-based dimension-reduced k -means clustering methods outperform the original k -means clustering with the full feature dimension. Therefore, it is useful to carry out dimension reduction before k -means clustering for large datasets.

3.2.3 MNIST

Figure 3 shows the performance of PCA-assisted, UMAP-assisted and t-SNE-assisted clustering of the MNIST dataset. The sample size of the MNIST dataset is 70000, which has 784 features with 10 different digit labels. For each case, the dataset was reduced to dimension 2 using default parameters, and the plots were colored with the ground truth of the MNIST dataset. In Figure 3, by applying the UMAP algorithm, the clear clusters can be detected for the MNIST dataset. The t-SNE offers a reasonable clustering at dimension 2 too. However, the PCA does not provide a good clustering.

Table 4: Accuracy of K -means clustering of the Facebook Network without applying any reduction algorithms, as well as the accuracy of K -means assisted by PCA, UMAP and t-SNE with different dimensional reduction ratio. The sample size, feature size, and the number of labels of the Facebook Network are 22470, 22470, and 4, respectively.

Dataset	K -means accuracy w/o reduction	Reduced dimension	PCA accuracy	UMAP accuracy	t-SNE accuracy
Facebook Network (22470, 22470, 4)	0.374	11235 (1/2)	0.331	0.306	0.306
		5617 (1/4)	0.331	0.307	0.299
		2808 (1/8)	0.331	0.411	0.314
		1404 (1/16)	0.331	0.397	0.313
		702 (1/32)	0.331	0.401	0.306
		351 (1/64)	0.331	0.400	0.308
		224 (1/100)	0.331	0.400	0.327
		112 (1/200)	0.331	0.400	0.306
		44 (1/500)	0.331	0.400	0.313
		22 (1/1000)	0.331	0.401	0.306
		3	0.332	0.351	0.344
2	0.358	0.345	0.427		

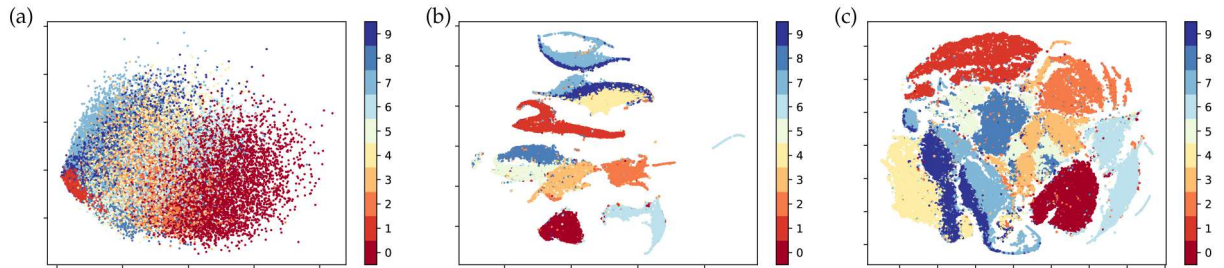


Figure 3: Comparison of different dimensional reduction algorithms on the MNIST dataset. Total 10 different labels are in the MNIST dataset, and we use the ground truth label to color each data points. (a) Feature size is reduced to dimension 2 by PCA. (b) Feature size is reduced to dimension 2 by t-SNE. (c) Feature size is reduced to dimension 2 by UMAP.

Table 5: Accuracy of k -NN of the MNIST dataset without applying any reduction algorithms, as well as the accuracy of k -NN assisted by PCA, UMAP and t-SNE with different dimensional reduction ratio. The sample size, feature size, and the number of labels of the MNIST dataset are 70000, 784, and 10, respectively.

Dataset	k -NN accuracy w/o reduction	Reduced dimension	PCA accuracy	UMAP accuracy	t-SNE accuracy
MNIST (70000, 784, 10)	0.948	392 (1/2)	0.951	0.937	0.696
		196 (1/4)	0.956	0.938	0.846
		98 (1/8)	0.960	0.937	0.893
		49 (1/16)	0.961	0.937	0.886
		24 (1/32)	0.953	0.937	0.842
		12 (1/64)	0.926	0.937	0.676
		7 (1/100)	0.846	0.936	0.940
		3	0.513	0.929	0.938
		2	0.323	0.919	0.928

Table 5 shows the accuracy of k -NN clustering of the MNIST dataset assisted by PCA, t-SNE, and UMAP with different dimensional reduction ratios. For each algorithm, we use the same settings as the Coil 20 dataset. Without applying any dimensional reduction algorithms, the accuracy of k -NN is 0.948. By applying PCA/UMAP with the reduction ratio greater than 1/64, the accuracy of PCA/UMAP-assisted

Table 6: Accuracy of K -means clustering of the MNIST dataset without applying any reduction algorithms, as well as the accuracy of K -means assisted by PCA, UMAP and t-SNE with different dimensional reduction ratio. The sample size, feature size, and the number of labels of the MNIST dataset are 70000, 784, and 10, respectively.

Dataset	K -means accuracy w/o reduction	Reduced dimension	PCA accuracy	UMAP accuracy	t-SNE accuracy
MNIST (70000, 784, 10)	0.494	392 (1/2)	0.487	0.665	0.122
		196 (1/4)	0.492	0.667	0.113
		98 (1/8)	0.498	0.673	0.113
		49 (1/16)	0.496	0.718	0.113
		24 (1/32)	0.501	0.697	0.114
		12 (1/64)	0.489	0.682	0.138
		7 (1/100)	0.464	0.677	0.740
		3	0.365	0.727	0.537
		2	0.300	0.712	0.593

k -NN is at the same level without using any dimensional reduction algorithm. However, in contract with UMAP and t-SNE, when the reduced dimension is 2 or 3, PCA performs poorly. This indicates that the PCA may not be suitable for dimension-reduction for datasets with a large sample size.

Table 6 describes the accuracy of K -means clustering of the MNIST dataset assisted by PCA, UMAP, and t-SNE with different dimensional reduction ratios. By applying PCA, the accuracy of K -means is around 0.45. The t-SNE method performance is quite unstable, from very poor (0.113) to the best (0.740), and to a relatively low value of 0.593. In contrast, we can see a stable and improved accuracy from using UMAP at various reduction ratios, indicating that the reduced feature generated by UMAP can better represent the clustering properties of the MNIST dataset compared to the PCA and t-SNE.

As observed early, the present UMAP and t-SNE-assisted k -means clustering methods also significantly out-perform the original k -means clustering for this dataset.

3.2.4 Jaccard distanced-based MNIST

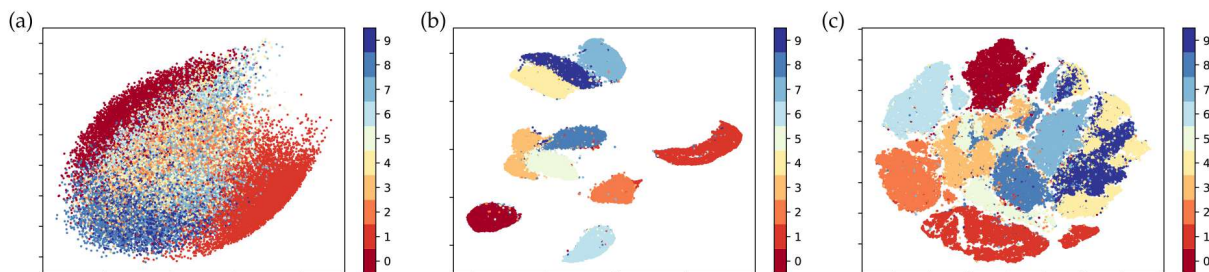


Figure 4: Comparison of different dimensional reduction algorithms on the Jaccard distanced-based MNIST dataset. Total 10 different labels are in the Jaccard distanced-based MNIST dataset, and we use the ground truth label to color each data points. (a) Feature size is reduced to dimension 2 by PCA. (b) Feature size is reduced to dimension 2 by t-SNE. (c) Feature size is reduced to dimension 2 by UMAP.

Out last validation dataset is Jaccard distanced-based MNIST. This dataset can be treated as a test on the Jaccard distance-based data representation. Figure 4 shows the performance of PCA-assisted, UMAP-assisted, and t-SNE-assisted clustering of the Jaccard distanced-based MNIST dataset. The dataset was reduced to dimension 2 using default parameters for visualization, and the plots were colored with the ground truth of the Jaccard distanced-based MNIST dataset. From Figure 4, we can see that UMAP provides the clearest clusters compared to PCA and t-SNE when the dimension is reduced to 2. The performance of t-SNE is reasonable while PCA does not give a good clustering.

Table 7: Accuracy of k -NN of the Jaccard distanced-based MNIST dataset without applying any reduction algorithms, as well as the accuracy of k -NN assisted by PCA, UMAP and t-SNE with different dimensional reduction ratio. The sample size, feature size, and the number of labels of the Jaccard distanced-based MNIST dataset are 70000, 70000, and 10, respectively.

Dataset	k -NN accuracy w/o reduction	Reduced dimension	PCA accuracy	UMAP accuracy	t-SNE accuracy
Jaccard distanced-based MNIST (70000, 70000, 10)	0.958	7000 (1/10)	0.958	0.958	NA
		3500 (1/20)	0.958	0.966	NA
		1750 (1/40)	0.958	0.967	NA
		875 (1/80)	0.958	0.967	NA
		437 (1/160)	0.958	0.968	0.718
		218 (1/320)	0.958	0.968	0.701
		109 (1/640)	0.958	0.968	0.873
		70 (1/1000)	0.958	0.968	0.915
		35 (1/2000)	0.956	0.968	0.872
		17 (1/5000)	0.938	0.968	0.916
		7 (1/10000)	0.867	0.967	0.942
		3	0.487	0.965	0.939
		2	0.313	0.960	0.924

Table 8: Accuracy of K -means clustering of the Jaccard distanced-based MNIST dataset without applying any reduction algorithms, as well as the accuracy of K -means assisted by PCA, UMAP and t-SNE with different dimensional reduction ratio. The sample size, feature size, and the number of labels of the Jaccard distanced-based MNIST dataset are 70000, 70000, and 10, respectively.

Dataset	K -means accuracy w/o reduction	Reduced dimension	PCA accuracy	UMAP accuracy	t-SNE accuracy
Jaccard distanced-based MNIST (70000, 70000, 10)	0.555	7000 (1/10)	0.436	0.329	NA
		3500 (1/20)	0.436	0.693	NA
		1750 (1/40)	0.436	0.792	NA
		875 (1/80)	0.435	0.793	NA
		437 (1/160)	0.435	0.793	0.114
		218 (1/320)	0.435	0.793	0.156
		109 (1/640)	0.435	0.794	0.114
		70 (1/1000)	0.436	0.793	0.113
		35 (1/2000)	0.435	0.794	0.116
		17 (1/5000)	0.436	0.793	0.113
		7 (1/10000)	0.431	0.793	0.737
		3	0.364	0.798	0.635
		2	0.261	0.791	0.635

Table 7 shows the accuracy of k -NN clustering of Jaccard distanced-based MNIST assisted by PCA, t-SNE, and UMAP with different dimensional reduction ratios. For each algorithm, we use the same settings as the Coil 20 dataset. Notably, the k -NN accuracy for the data without applying any dimensional reduction algorithm is 0.958, which is at the same level as the PCA algorithm with a reduction ratio greater than 1/5000. Moreover, we can find that UMAP performs well compared to PCA and t-SNE, indicating that after applying UMAP, the reduced feature still preserves most of the valued information of the Jaccard distanced-based MNIST dataset. The stability and persistence of UMAP at various reduction ratios are the most important features.

Table 8 describes the accuracy of K -means clustering of the Jaccard distanced-based MNIST dataset assisted by PCA, UMAP, and t-SNE with different dimensional reduction ratio. For consistency, we will use the same standard parameters as k -NN. Similar to the MNIST dataset, the accuracy of K -means clustering

assisted by UMAP still has the best performance. When the reduced dimension is 3, UMAP will result in the highest K -means accuracy 0.798. Noticeably, although PCA performs well on k -NN accuracy, it has the lowest K -mean accuracy, indicating that PCA is not a suitable dimensional reduction algorithm, especially for those datasets with a large number of samples. To be noted, the t-SNE accuracy at four reduced dimensions are not available due to the extremely long running time.

In a nutshell, PCA, UMAP, and t-SNE can all perform well for k -NN. However, for the Coil 20 dataset, UMAP performs slightly poorly, whereas the t-SNE performs well, which may be caused by a lack of data size. In order to train UMAP, it needs a suitable data size. The Coil 20 dataset has 20 labels, each with only 72 samples. This may not be enough to train UMAP properly. However, even in this case, UMAP performance is still very stable at various reduction ratios and is the best method in terms of reliability, which become the major advantages of UMAP. Another strength of UMAP comes from its dimension-reduction for K -means clustering. In most cases, UMAP can improve K -means clustering accuracy, especially for the Jaccard distanced-based MNIST dataset. Furthermore, UMAP can generate a very clear and elegant visualization of clusters with low dimensional reduction value such as 2. Additionally, UMAP performed better than PCA and t-SNE for a larger dataset (MNIST and Jaccard distanced-based MNIST). Especially for the Jaccard distanced-based MNIST data, where Jaccard distance was used as the metric, UMAP performed best, which indicates the merit of using UMAP for Jaccard distanced-based datasets, such as COVID-19 SNP datasets. Furthermore, the accuracies for k -NN classification and K -means clustering are both improved on the Jaccard distance-based MNIST dataset compared to the original MNIST dataset, which provides convincing evidence that the Jaccard distance representation will help improve the performance of the clustering on the SARS-CoV-2 mutation dataset in the following sections.

3.3 Efficiency comparison

It is important to understand the computational time behaviors of various methods. To this end, we compare computational time for three dimension-reduction techniques. Figure 5 depicts the computational time of three methods for the four datasets under various reduction ratios. The green, orange, and blue lines represent the computational time of t-SNE, UMAP, and PCA, respectively. Some points in green line of Figure 5 (d) are not available, which due to the extremely long running time. PCA performed best in most cases, except for the Coil 20 dataset, where UMAP had comparable computational time. This behavior is expected because PCA is a linear transformation, and its time should scale linearly with the number of components in the lower dimensional space. UMAP and t-SNE were slower than PCA, but it is evident from MNIST and Jaccard distanced-based MNIST datasets that UMAP scales better with the increase in the number of samples. Note that for Jaccard distanced-based MNIST, a higher dimension was not computed because the computational time was too long. For Facebook Network, UMAP is outperforming t-SNE; however, for higher dimensions, t-SNE computed faster. Nonetheless, from our baseline test Table 3, t-SNE does not perform well, indicating instability. Faster computation time may indicate too fast of a convergence, which leads to poor embedding.

4 SARS-CoV-2 mutation clustering

4.1 World SARS-CoV-2 mutation clustering

We gather data submitted to GISAID up to October 30, 2020, and the total number of samples is 89627. We first get the SNP information by applying the multiple sequence alignment, which leads to 23763 unique SNPs. Next, we calculate the pairwise Jaccard distance of our dataset in order to generate the Jaccard distance-based features. Here, the number of rows is the number of samples (89627), and the number of columns is the feature size (89627). As we mentioned in Section 2.3, the Jaccard distance-based feature is

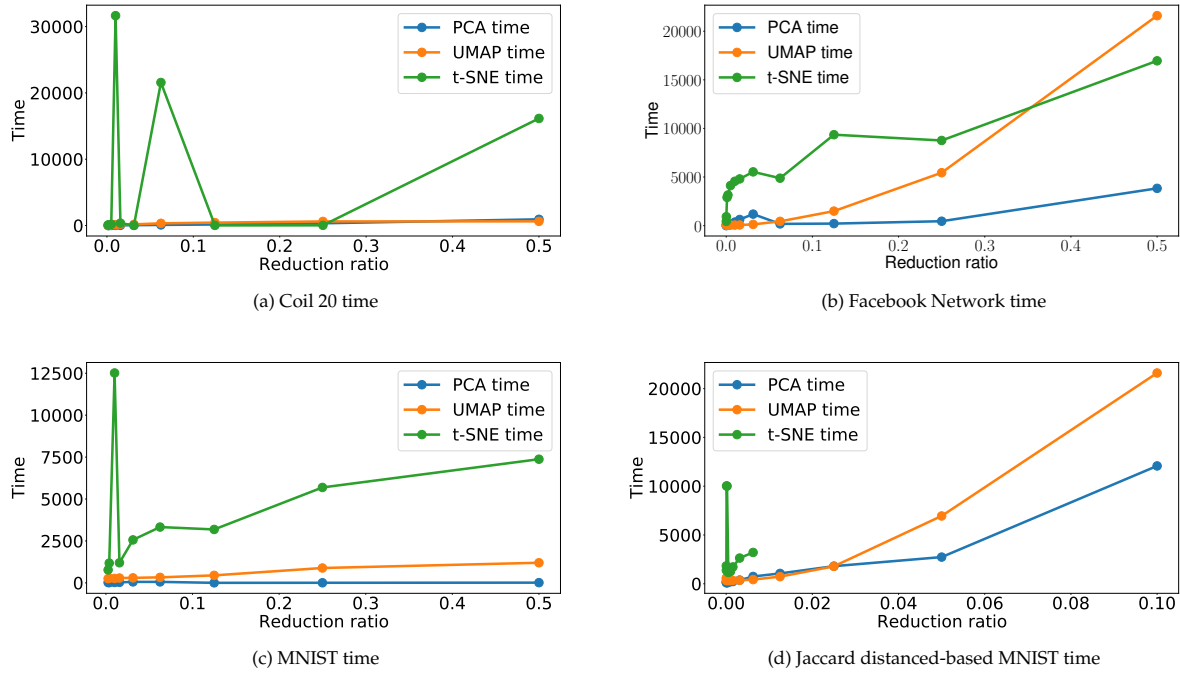


Figure 5: Computational time of each reduction ratio. The green, orange and blue lines represent the computational time of t-SNE, UMAP, and PCA, respectively. Not surprisingly, PCA performs the best in the majority of cases, except for the Coil 20 dataset. UMAP and t-SNE perform worse than PCA, but UMAP scales better when there are more samples, as evident from MNIST and Jaccard distanced-based MNIST datasets. Note that for Jaccard distanced-based MNIST, the higher dimension was not computed because the computational time was too long.

a square matrix. However, due to the large size of samples and features, applying K -means clustering directly on the feature of the size of 89627×89627 is a very time-consuming process. Considering that UMAP outperforms the other two dimensional reduction algorithms (PCA and t-SNE) on the Jaccard distance-based MNIST dataset, we employ UMAP to reduce our original feature with the size of 89627×89627 to 89627×200 . To be noted, UMAP is a reliable and stable algorithm, which performs consistently in clustering at various reduction ratios. Therefore, there is no need to use the same reduction dimension of 200 and one can also choose a different reduction dimension value to generate similar results.

With the reduced dimension feature that has the size of 89627×200 , we split our SARS-CoV-2 dataset into different clusters by applying the K -means clustering methods. After comparing the WCSS under a different number of clusters, we find that there are 6 clusters forming within the SARS-CoV-2 population based on the elbow method. Table 11 shows the top 25 single mutations of each cluster. In order to understand the relationship, we also analyzed the commutation occurring in each cluster (Table 9). From Table 11 and Table 9 we see the following:

Table 9: The frequency and occurrence percentage of SARS-CoV-2 co-mutations from each clusters in the world.

Cluster	Co-mutations	Frequency	Occurrence percentage
Cluster 1	[241, 1163, 3037, 7540, 14408, 16647, 18555, 22992, 23401, 23403, 28881, 28882, 28883]	776	0.463
Cluster 2	[241, 3037, 14408, 23403]	8640	0.925
Cluster 3	[241, 1059, 3037, 14408, 23403, 25563]	8878	0.662
Cluster 4	[241, 3037, 14408, 23403, 28881, 28882, 28883]	14913	0.829
Cluster 5	[241, 3037, 14408, 23403]	17412	0.969
Cluster 6	[241, 1163, 3037, 7540, 14408, 16647, 18555, 22992, 23401, 23403, 28881, 28882, 28883]	1352	0.771

- Though Clusters 1 and 6 seem similar from the top 25 single mutations, the co-mutations tells a different story. The same co-mutations have a higher frequency in Cluster 6, indicating that the co-mutation has higher number of descendants.

- Clusters 2 and 5 have high frequency of [241, 3037, 14408, 23403] mutations, but Cluster 5 has a clear co-mutation descendent with high frequency.
- Cluster 3 has a unique combination of mutation that is only popular in Cluster 3.

Table 12 shows the cluster distributions of samples from 25 countries. Here, we use the ISO 3166-1 alpha-2 codes as the country code. The listed countries are the United Kingdom (UK), the United States (US), Australia (AU), India (IN), Switzerland (CH), Netherlands (NL), Canada (CA), France (FR), Belgium (BE), Singapore (SG), Spain (ES), Russia (RU), Portugal (PT), Denmark (DK), Sweden (SE), Austria (AT), Japan (JP), South Africa (ZA), Iceland (IS), Brazil (BR), Saudi Arabia (SA), Norway (NO), China (CN), Italy (IT), and Korea (KR). From Table 12, we can see the following:

- SNP profiles from UK are dominated in Clusters 5 and 4.
- Clusters 1 and 6’s SNP profiles are predominantly found in AU.
- SNP profiles from US are found mostly in Clusters 3 and 5.
- Most country’s SNP profiles are found in Clusters 2 - 5, with some having slightly higher numbers, but not as significant as the UK, US and AU.

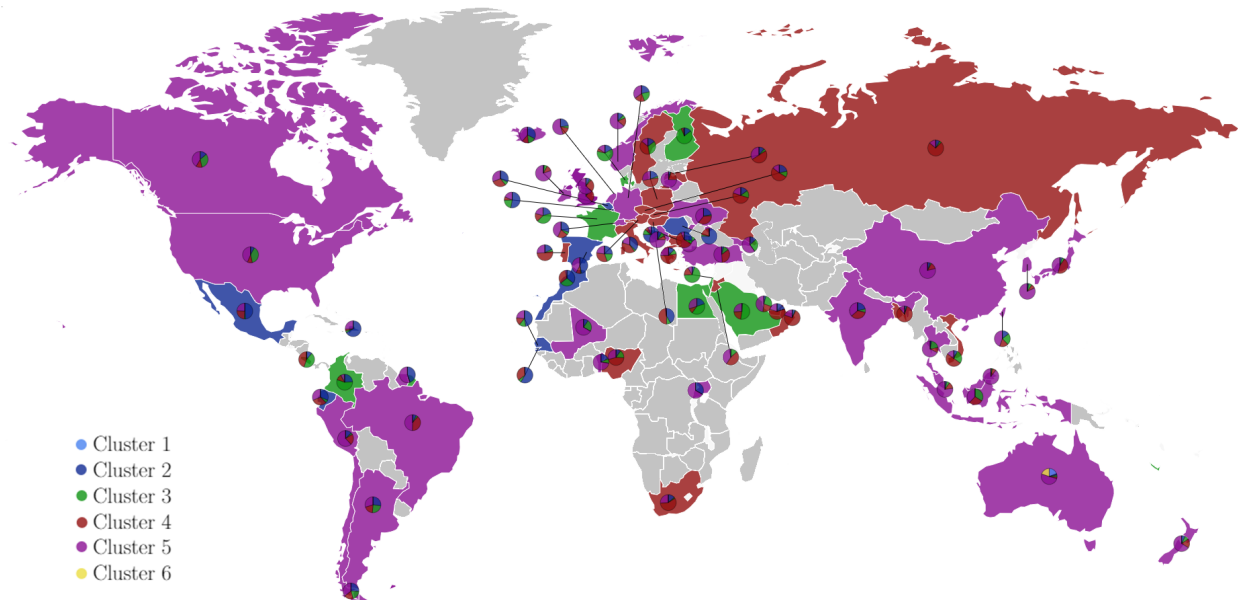


Figure 6: Cluster distribution of the global SARS-CoV-2 mutation dataset. Using Highchart, the world map was colored, according to the dominant cluster. Clusters 1, 2, 3, 4, 5, and 6 were colored with light blue, blue, green, red, purple and yellow, respectively. For example, United States have SNP profiles from all clusters, but Cluster 5 (purple) is the dominant type in the US. Only countries with more than 25 sequenced data available on GISAID were considered. Countries with fewer than 25 samples are labeled grayed.

Notably, in Table 9, Cluster 2 and Cluster 5 have the same co-mutations with a relatively large frequency, while Cluster 1 and Cluster 6 share the same co-mutations with a relatively low frequency, which indicate that Cluster 2 and Cluster 5 share the same “root” with a large size, while Cluster 1 and Cluster 6 share the same “root” with a smaller size in the 200-dimensional (200D) space. However, we cannot visualize the distribution of our reduced dataset in the 200D space. Therefore, benefit from the stable and reliable performance of UMAP at various reduction ratios, we reduce the dimension of our original dataset to 2, which enables us to observe the distribution of the dataset in the two-dimensional (2D) space. Figure 7 visualizes the distribution of our dataset with 6 distinct clusters with 2D UMAP. It can be seen that 2 clusters (i.e., Cluster 2’ and Cluster 3’) share a small “root” located in the middle of the figure, and Cluster 4’ and Cluster 5’ share another large “root” that also located in the middle of the figure.

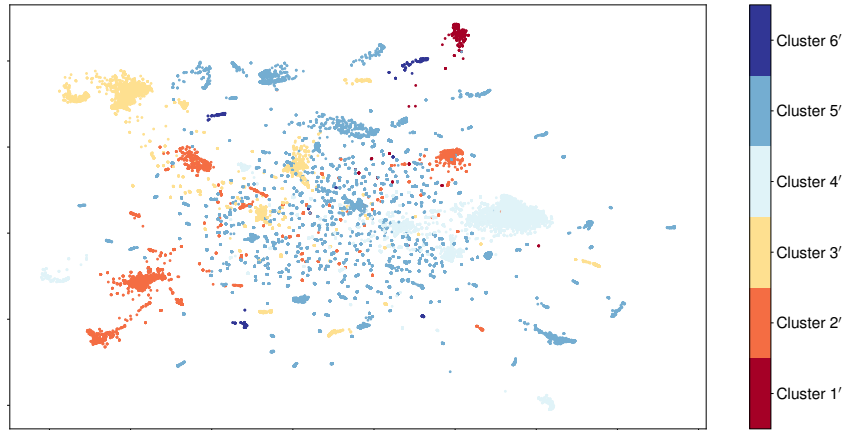


Figure 7: 2D UMAP visualization of the world SARS-CoV-2 mutation dataset with 6 distinct clusters. Red, orange, yellow, light blue, blue, and dark blue represent for Clusters 1', 2', 3', 4', 5', and 6', respectively.

4.2 United States SARS-CoV-2 mutation clustering

In addition to analyzing the clustering in the world, SNP profiles of SARS-CoV-2 from the United States (US) were considered. In this section, the US dataset has 10279 unique single mutations and 22390 samples. Therefore, the dimension of the Jaccard distance-based dataset is 22390×22390 . After applying the UMAP, we reduce the dimension of the original dataset to be 22390×200 . Following the similar K -means clustering processes as we did for the world dataset, we find that there are 6 predominant clusters forming in the United States. Figure 8 show the US map with the cluster statistic. Here, Highchart was used to generate the plot with the pie chart. Each states were colored based on the dominant cluster.

Table 13 shows the top 25 mutations from each clusters in the United States. The states with more than 50 samples are listed. Table 10 shows the common occurring co-mutations, and we can observe the following:

- Cluster F have high frequency of co-mutations [241, 3037, 14408, 23403, 28881, 28882, 28883], which is a descendent of common co-mutations of Cluster 4 [241, 3037, 14408, 23403, 28881, 28882, 28883] from Table 13.
- Clusters A, B, C, and D have frequent co-mutations [241, 1059, 3037, 14408, 23403, 25563], which are also frequent co-mutations of Cluster 3.

Table 10: The frequency and occurrence percentage of SARS-CoV-2 co-mutations from each clusters in US clusters.

Cluster	Co-mutations	Frequency	Occurrence percentage
Cluster A	[241, 1059, 3037, 14408, 23403, 25563]	3116	0.465
Cluster B	[241, 1059, 3037, 14408, 23403, 25563]	5763	0.605
Cluster C	[241, 1059, 3037, 14408, 23403, 25563]	8878	0.662
Cluster D	[241, 1059, 3037, 14408, 23403, 25563, 27964]	1225	0.864
Cluster E	[8782, 17747, 17858, 18060, 28144]	1109	0.743
Cluster F	[241, 3037, 14408, 23403, 28881, 28882, 28883]	2575	0.932

Notably, in Table 10, Clusters A, B, and C have the same high-frequency co-mutations, indicating that these three clusters may share the same “root” in the 200D space. However, it is impossible to show the distribution of each cluster in the 200D space. Considering the stability and reliability of UMAP at various reduction ratios, we employ UMAP to the original US dataset with reduced dimension 2, aiming to observe the distribution of the dataset in the 2D space. Figure 9 illustrates the 2D visualization of the US dataset

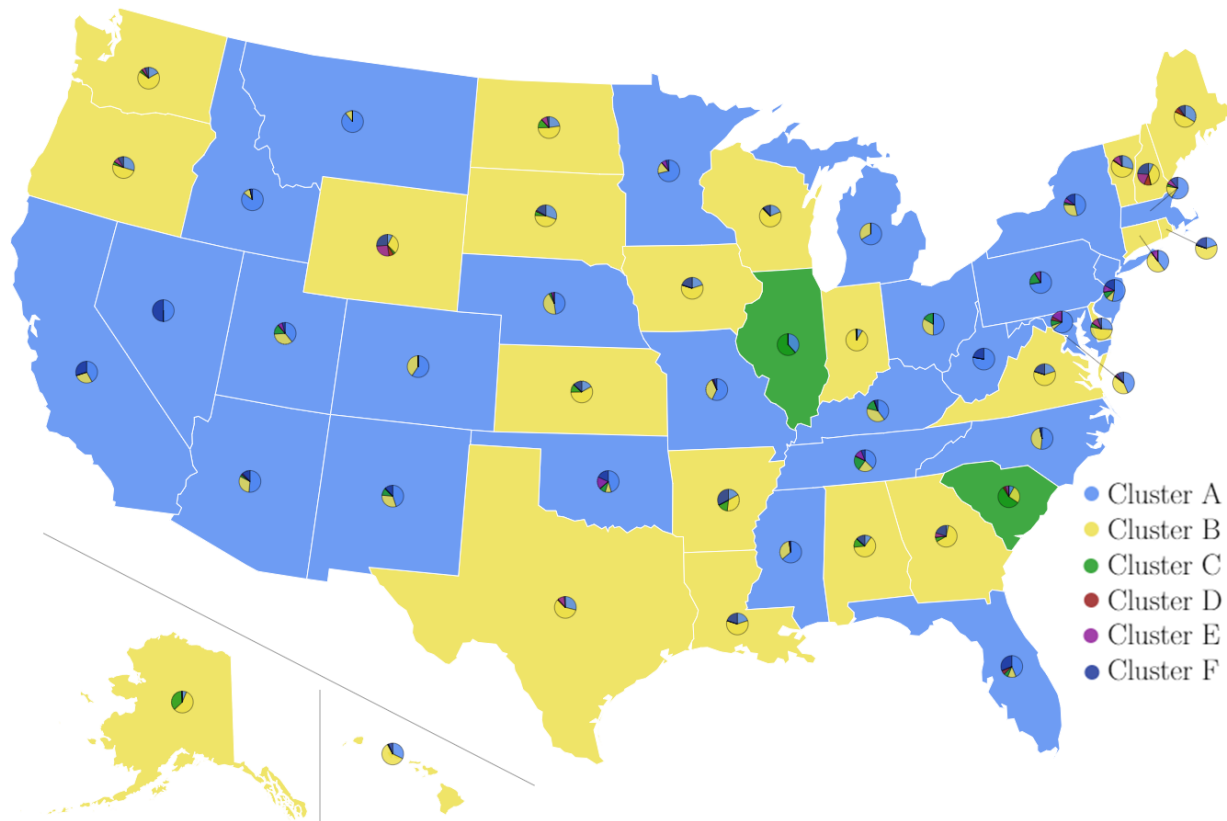


Figure 8: Cluster distribution of United States SARS-CoV-2 mutation dataset. Using Highchart, the US map was colored, according to the dominant cluster. Clusters A, B, C, D, E, and F were colored with light blue, blue, green, red, purple, and yellow, respectively. For example, United States have SNP profiles from all clusters, but Cluster E (purple) is the dominant type in the US. Only those countries that have more than 25 sequenced data available on GISAID were considered in the plot.

with 6 distinct clusters. We can see that there are 3 clusters (Clusters A', B', and F') share the same "root" located in the middle of the figure, while the other 3 clusters (Clusters C', D', and E') are not. This confirms our deduction about why Clusters A, B, and C have the same high-frequency co-mutations in Table 10.

5 Discussion

In this section, we compared our past results [31] with our new method to gain a different perspective in clustering with the SNP profiles of COVID-19. In our previous work, a total of 8309 unique single mutations are detected in 15140 SARS-CoV-2 isolates. Here, we also calculate the pairwise distance among 15140 SNP profiles and set the number of clusters to be six. Table 15 shows the cluster distribution of samples from the 15 countries [31]. The listed countries are the United States (US), Canada (CA), Australia (AU), United Kingdom (UK), Germany (DE), France (FR), Italy (IT), Russia (RU), China (CN), Japan (JP), Korean (KR), India (IN), Spain (ES), Saudi Arabia (SA), and Turkey (TR), and we use Cluster I, II, III, IV, V, and VI to represent six clusters without applying any dimensional reduction algorithm. Table 16 lists the cluster distribution of samples from the same 15 countries, where we use I_p , II_p , III_p , IV_p , V_p , and VI_p to represent six clusters performed by PCA with the reduction ratio to be 1/160. Table 17 lists the cluster distribution of samples from the same 15 countries, where we use I_u , II_u , III_u , IV_u , V_u , and VI_u to represent six clusters performed by UMAP with the reduction ratio setting to be 1/160. Noticeably, the SNP profile is focused in Cluster I_u , whereas in the non-reduced version, the samples are more spread out. This may be caused by the large number of features, making computed distance between the centroid and each data too similar, and leading to samples being placed in incorrect clusters.

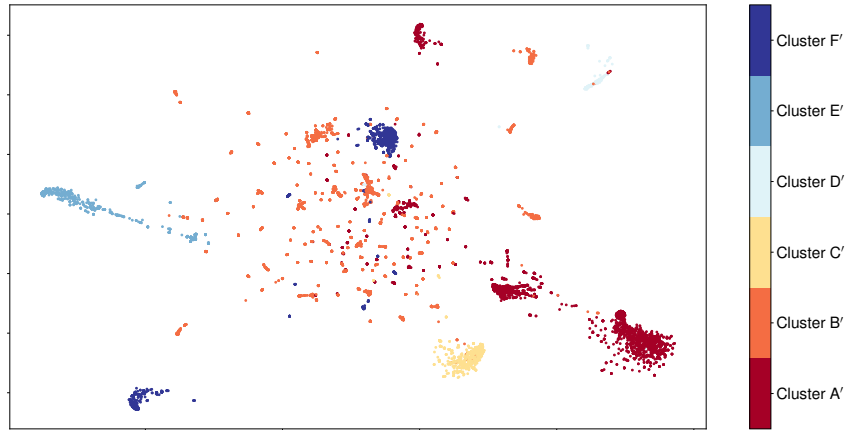


Figure 9: The 2D UMAP visualization of the US SARS-CoV-2 mutation dataset with 6 distinct clusters. Red, orange, yellow, light blue, blue, and dark blue represent for Cluster A', B', C', D', E', and F', respectively.

Not surprisingly, PCA and the original method for [31] has nearly identical result. It has been shown in [31] that PCA is the continuous solution of the cluster indicators in the K -means clustering method. On the other hand, UMAP shows a slightly different result. In the PCA method, the distribution is more spread out. In addition, the top occurrence for each country is higher for UMAP. On the other hand, we see that there are more samples in Cluster I_u for UMAP, which may indicate that mutations in Cluster I_u are the main strand.

Moreover, Figure 10 illustrates the 2D visualizations of the US dataset up to June 01, 2020, with 6 distinct clusters by applying two different dimensional reduction algorithms. We can see that the data distribute disorderly under both PCA- and UMAP-assisted K -means clustering algorithms. Specifically, the PCA-assisted algorithm has a really poor clustering performance, while the UMAP-assisted algorithm forms more clear and better clusters than the PCA-assisted algorithm, which is consistent with our previous analysis in Section 3.1.

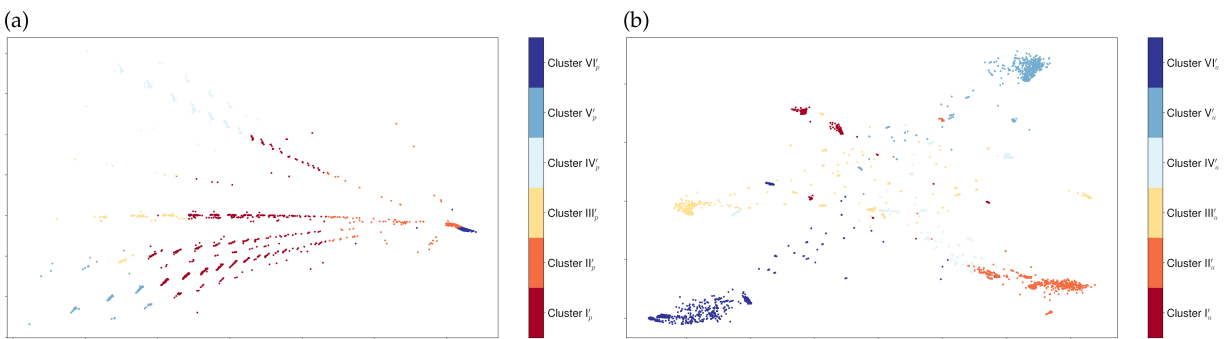


Figure 10: 2D visualizations of the US SARS-CoV-2 mutation dataset up to June 01, 2020 with 6 distinct clusters by applying two different dimensional reduction algorithms. (a) 2D PCA visualization. Red, orange, yellow, light blue, blue, and dark blue represent for Cluster I'_p , II'_p , III'_p , IV'_p , V'_p , and VI'_p , respectively. (b) 2D UMAP visualization. Red, orange, yellow, light blue, blue, and dark blue represent for Cluster I'_u , II'_u , III'_u , IV'_u , V'_u , and VI'_u , respectively.

6 Conclusion

The rapid global spread of coronavirus disease 2019 (COVID-19) caused by severe acute respiratory syndrome coronavirus 2 (SARS-CoV-2) has led to genetic mutation stimulated by genetic evolution and adaptation. Up to October 30, 89627 complete SARS-CoV-2 sequences, and a total of 23763 unique SNPs have been detected. Our previous work traced the COVID-19 transmission pathways and analyzed the distribution of the subtypes of SARS-CoV-2 across the world based on 15,140 complete SARS-CoV-2 sequences. The K -means clustering separated the sequences into six distinguished clusters. However, considering the tremendous increase in the number of available SARS-CoV-2 sequences, an efficient and reliable dimensional reduction method is urgently required. Therefore, the objective of the present work is to explore the best suited dimension reduction algorithm based on their performance and effectiveness. Here, a linear algorithm PCA and two non-linear algorithms, t-distributed stochastic neighbor embedding (t-SNE) and uniform manifold approximation and projection (UMAP), have been discussed. To evaluate the performance of dimension reduction techniques in clustering, which is an unsupervised problem, we first cast classification problems into clustering problems with labels. Next, by setting different reduction ratios, we test the effectiveness and accuracy of PCA, t-SNE, and UMAP for k -NN and K -means using four benchmark datasets. The results show that overall, UMAP outperforms other two algorithms. The major strengths of UMAP is that UMAP-assisted k -NN classification and UMAP-assisted K -means clustering at various dimension reduction ratios have a consistent performance in terms of accuracy, which proves that UMAP is a stable and reliable dimension reduction algorithm. Moreover, compared to the K -means clustering accuracy that does not involve any dimensional reduction, UMAP-assisted K -means clustering can improve the accuracy for most cases. Furthermore, when the dimension is reduced to two, the UMAP clustering visualization is clear and elegant. Additionally, UMAP is a relatively efficient algorithm compared to t-SNE. Although PCA is a faster algorithm, its major limitation is its poor performance in accuracy. To be noted, UMAP performs better than PCA and t-SNE for the dataset with a large number of samples, indicating it is the best suited dimensional reduction algorithm for our SARS-CoV-2 mutation dataset. Moreover, we apply the UMAP-assisted K -means clustering to the world SARS-CoV-2 mutation dataset (up to October 30, 2020), which displays six distinct clusters. Correspondingly, the same approaches are also applied to the United States SARS-CoV-2 mutation dataset (up to October 30, 2020), resulting in six different clusters as well. Furthermore, we provide a new perspective by utilizing UMAP-assisted K -means clustering to analyze our previous SARS-CoV-2 mutation datasets, and the 2D visualization of UMAP-assisted K -means clustering of our previous world SARS-CoV-2 mutation dataset (up to June 01, 2020) forms more clear clusters than the PCA-assisted K -means clustering. Finally, one of our four datasets was generated by the Jaccard distance representation, which improves both k NN classification and k -means clustering accuracies on the original dataset.

Acknowledgment

This work was supported in part by NIH grant GM126189, NSF Grants DMS-1721024, DMS-1761320, and IIS1900473, Michigan Economic Development Corporation, Bristol-Myers Squibb, and Pfizer. The authors thank The IBM TJ Watson Research Center, The COVID-19 High Performance Computing Consortium, and NVIDIA for computational assistance.

References

- [1] Weekly operational update on COVID-19, 30 october 2020, 2020.
- [2] I. Alam, A. A. Kamau, M. Kulmanov, L. Jaremko, S. T. Arold, A. Pain, T. Gojobori, and C. M. Duarte. Functional pangenome analysis shows key features of e protein are preserved in sars and SARS-CoV-2. *Frontiers in cellular and infection microbiology*, 10:405, 2020.
- [3] Y. Bai, D. Jiang, J. R. Lon, X. Chen, M. Hu, S. Lin, Z. Chen, X. Wang, Y. Meng, and H. Du. Comprehensive evolution and molecular characteristics of a large number of SARS-CoV-2 genomes reveal its epidemic trends. *International Journal of Infectious Diseases*, 100:164–173, 2020.
- [4] E. Becht, L. McInnes, J. Healy, C.-A. Dutertre, I. W. Kwok, L. G. Ng, F. Ginhoux, and E. W. Newell. Dimensionality reduction for visualizing single-cell data using umap. *Nature biotechnology*, 37(1):38–44, 2019.
- [5] M. Belkin and P. Niyogi. Laplacian eigenmaps and spectral techniques for embedding and clustering. *Advances in neural information processing systems*, 14:585–591, 2001.
- [6] J. Chen, R. Wang, M. Wang, and G.-W. Wei. Mutations strengthened SARS-CoV-2 infectivity. *arXiv preprint arXiv:2005.14669*, 2020.
- [7] J. Chen, R. Zhao, Y. Tong, and G.-W. Wei. Evolutionary de Rham-Hodge method. *arXiv preprint arXiv:1912.12388*, 2019.
- [8] M. A. Cox and T. F. Cox. Multidimensional scaling. In *Handbook of data visualization*, pages 315–347. Springer, 2008.
- [9] P. Forster, L. Forster, C. Renfrew, and M. Forster. Phylogenetic network analysis of SARS-CoV-2 genomes. *Proceedings of the National Academy of Sciences*, 117(17):9241–9243, 2020.
- [10] Y.-N. Gong, K.-C. Tsao, M.-J. Hsiao, C.-G. Huang, P.-N. Huang, P.-W. Huang, K.-M. Lee, Y.-C. Liu, S.-L. Yang, R.-L. Kuo, et al. SARS-CoV-2 genomic surveillance in Taiwan revealed novel ORF8-deletion mutant and clade possibly associated with infections in middle east. *Emerging Microbes & Infections*, 9(1):1457–1466, 2020.
- [11] I. T. Jolliffe and J. Cadima. Principal component analysis: a review and recent developments. *Philosophical Transactions of the Royal Society A: Mathematical, Physical and Engineering Sciences*, 374(2065):20150202, 2016.
- [12] S. M. Kasibhatla, M. Kinikar, S. Limaye, M. M. Kale, and U. Kulkarni-Kale. Understanding evolution of SARS-CoV-2: A perspective from analysis of genetic diversity of rdrp gene. *Journal of Medical Virology*, 2020.
- [13] Y. LeCun, L. Bottou, Y. Bengio, and P. Haffner. Gradient-based learning applied to document recognition. *Proceedings of the IEEE*, 86(11):2278–2324, 1998.
- [14] M. Levandowsky and D. Winter. Distance between sets. *Nature*, 234(5323):34–35, 1971.
- [15] X. Li, J. Zai, Q. Zhao, Q. Nie, Y. Li, B. T. Foley, and A. Chaillon. Evolutionary history, potential intermediate animal host, and cross-species analyses of SARS-CoV-2. *Journal of medical virology*, 92(6):602–611, 2020.
- [16] G. C. Linderman, M. Rachh, J. G. Hoskins, S. Steinerberger, and Y. Kluger. Fast interpolation-based t-SNE for improved visualization of single-cell rna-seq data. *Nature methods*, 16(3):243–245, 2019.
- [17] L. v. d. Maaten and G. Hinton. Visualizing data using t-SNE. *Journal of machine learning research*, 9(Nov):2579–2605, 2008.

- [18] L. McInnes, J. Healy, and J. Melville. Umap: Uniform manifold approximation and projection for dimension reduction. *arXiv preprint arXiv:1802.03426*, 2018.
- [19] S. A. Nene, S. K. Nayar, and H. Murase. Columbia object image library (COIL-20), 1996.
- [20] C. S. G. of the International et al. The species severe acute respiratory syndrome-related coronavirus: classifying 2019-ncov and naming it SARS-CoV-2. *Nature Microbiology*, 5(4):536, 2020.
- [21] R. D. Page. Space, time, form: viewing the tree of life. *Trends in Ecology & Evolution*, 27(2):113–120, 2012.
- [22] B. Rozemberczki, C. Allen, and R. Sarkar. Multi-scale attributed node embedding. 2019.
- [23] J. W. Sammon. A nonlinear mapping for data structure analysis. *IEEE Transactions on computers*, 100(5):401–409, 1969.
- [24] F. Sievers, A. Wilm, D. Dineen, T. J. Gibson, K. Karplus, W. Li, R. Lopez, H. McWilliam, M. Remmert, J. Söding, et al. Fast, scalable generation of high-quality protein multiple sequence alignments using Clustal Omega. *Molecular systems biology*, 7(1):539, 2011.
- [25] D. I. Spivak. Metric realization of fuzzy simplicial sets. *Self published notes, available online at <https://www.semanticscholar.org/paper/METRIC-REALIZATION-OF-FUZZY-SIMPLICIAL-SETS-Spivak/a73fb9d562a3850611d2615ac22c3a8687fa745e>*, 2012.
- [26] J. Tang, J. Liu, M. Zhang, and Q. Mei. Visualizing large-scale and high-dimensional data. In *Proceedings of the 25th international conference on world wide web*, pages 287–297, 2016.
- [27] Y. Toyoshima, K. Nemoto, S. Matsumoto, Y. Nakamura, and K. Kiyotani. SARS-CoV-2 genomic variations associated with mortality rate of COVID-19. *Journal of human genetics*, pages 1–8, 2020.
- [28] D. Ulyanov. Multicore-TSNE. <https://github.com/DmitryUlyanov/Multicore-TSNE>, 2016.
- [29] L. van Dorp, M. Acman, D. Richard, L. P. Shaw, C. E. Ford, L. Ormond, C. J. Owen, J. Pang, C. C. Tan, F. A. Boshier, et al. Emergence of genomic diversity and recurrent mutations in SARS-CoV-2. *Infection, Genetics and Evolution*, page 104351, 2020.
- [30] R. Wang, J. Chen, K. Gao, Y. Hozumi, C. Yin, and G.-W. Wei. Characterizing SARS-CoV-2 mutations in the United States. *arXiv preprint arXiv:2007.12692*, 2020.
- [31] R. Wang, J. Chen, Y. Hozumi, C. Yin, and G.-W. Wei. Decoding asymptomatic COVID-19 infection and transmission. *The journal of physical chemistry letters*, 11:10007–10015, 2020.
- [32] R. Wang, Y. Hozumi, C. Yin, and G.-W. Wei. Decoding SARS-CoV-2 transmission, evolution and ramification on COVID-19 diagnosis, vaccine, and medicine. *arXiv preprint arXiv:2004.14114*, 2020.
- [33] G. Wei. Wavelets generated by using discrete singular convolution kernels. *Journal of Physics A: Mathematical and General*, 33(47):8577, 2000.
- [34] M. Worobey, J. Pekar, B. B. Larsen, M. I. Nelson, V. Hill, J. B. Joy, A. Rambaut, M. A. Suchard, J. O. Wertheim, and P. Lemey. The emergence of SARS-CoV-2 in Europe and North America. *Science*, 370(6516):564–570, 2020.
- [35] F. Wu, S. Zhao, B. Yu, Y.-M. Chen, W. Wang, Z.-G. Song, Y. Hu, Z.-W. Tao, J.-H. Tian, Y.-Y. Pei, et al. A new coronavirus associated with human respiratory disease in China. *Nature*, 579(7798):265–269, 2020.
- [36] T. Zhou, K. C. Chan, Y. Pan, and Z. Wang. An approach for determining evolutionary distance in network-based phylogenetic analysis. In *International Symposium on Bioinformatics Research and Applications*, pages 38–49. Springer, 2008.

7 Appendix

Table 11: Clusters distribution of the top 25 single mutations of SARS-CoV-2 in the world, collected up to October 30, 2020.

Top	Position	Cluster 1	Cluster 2	Cluster 3	Cluster 4	Cluster 5	Cluster 6
Top 1	23403	1676	9301	13355	17711	36351	1753
Top 2	14408	1676	9265	13392	17728	36306	1753
Top 3	3037	1676	9264	13350	17731	36342	1753
Top 4	241	1669	9065	13176	17549	36128	1380
Top 5	28881	1676	64	28	16509	14771	1753
Top 6	28882	1676	15	16	16508	14735	1753
Top 7	28883	1676	13	4	16513	14737	1753
Top 8	25563	0	24	13357	1022	7702	0
Top 9	1059	0	23	10919	72	4797	0
Top 10	22227	1	5	25	71	9211	0
Top 11	26801	6	15	14	97	9094	17
Top 12	21255	1	4	8	119	9101	0
Top 13	6286	0	20	5	66	9092	1
Top 14	29645	0	2	9	74	9069	0
Top 15	445	0	1	0	53	9057	0
Top 16	28932	0	16	10	52	9031	1
Top 17	1163	1676	4	0	271	4566	1753
Top 18	22992	1675	27	11	930	3292	1753
Top 19	11083	2	179	415	462	6046	32
Top 20	18555	1675	13	37	15	3216	1752
Top 21	16647	1676	5	9	3	3200	1753
Top 22	23401	1675	4	3	17	3192	1753
Top 23	7540	1676	0	0	3	3170	1753
Top 24	27944	0	1	5	49	6308	0
Top 25	204	6	6	11	15	5454	0

Table 12: Cluster distributions of SARS-CoV-2 sequences from top 25 countries with the highest number of sequences as of October 30, 2020. The top 25 countries are the United Kingdom (UK), the United States (US), Australia (AU), India (IN), Switzerland (CH), Netherlands (NL), Canada (CA), France (FR), Belgium (BE), Singapore (SG), Spain (ES), Russia (RU), Portugal (PT), Denmark (DK), Sweden (SE), Austria (AT), Japan (JP), South Africa (ZA), Iceland (IS), Brazil (BR), Saudi Arabia (SA), Norway (NO), China (CN), Italy (IT), and Korea (KR).

Top	Country	Cluster 1	Cluster 2	Cluster 3	Cluster 4	Cluster 5	Cluster 6
Top 1	UK	16	2926	1112	9530	22959	48
Top 2	US	1	1798	8620	2209	9760	0
Top 3	AU	1652	247	346	286	4328	1700
Top 4	IN	0	415	138	683	708	0
Top 5	CH	0	580	114	411	827	0
Top 6	NL	0	397	80	283	942	0
Top 7	CA	1	193	447	166	572	2
Top 8	FR	5	220	451	176	223	2
Top 9	BE	0	285	66	269	274	0
Top 10	SG	0	35	50	115	675	0
Top 11	ES	0	406	14	81	365	0
Top 12	RU	0	62	29	539	101	0
Top 13	PT	0	114	31	334	166	0
Top 14	DK	0	96	359	32	89	0
Top 15	SE	0	84	182	219	79	0
Top 16	AT	0	142	108	180	129	0
Top 17	JP	0	25	26	236	242	0
Top 18	ZA	0	72	11	299	134	0
Top 19	IS	0	137	67	54	162	0
Top 20	BR	0	30	14	154	194	0
Top 21	SA	0	5	193	81	98	0
Top 22	NO	0	42	23	61	224	0
Top 23	CN	0	18	8	43	258	0
Top 24	IT	0	120	11	129	66	0
Top 25	KR	0	10	21	26	260	0

Table 13: Clusters distribution of the top 25 single mutations of SARS-CoV-2 in the United States, collected up to October 30, 2020.

Top	Position	Cluster A	Cluster B	Cluster C	Cluster D	Cluster E	Cluster F
Top 1	23403	6686	8110	1418	486	3	2757
Top 2	14408	6688	8100	1418	486	3	2752
Top 3	3037	6674	8097	1417	486	2	2756
Top 4	241	6562	8033	1403	470	2	2695
Top 5	25563	4906	6405	1417	485	0	8
Top 6	1059	4235	5831	1417	485	1	3
Top 7	27964	4	1880	1402	0	1	1
Top 8	28881	16	408	2	2	1	2733
Top 9	28882	9	401	1	1	0	2732
Top 10	28883	0	399	0	1	0	2738
Top 11	28144	8	728	0	0	1486	2
Top 12	8782	1	728	0	0	1482	1
Top 13	18060	14	299	0	0	1469	8
Top 14	17858	3	296	0	0	1460	2
Top 15	17747	1	308	0	0	1420	3
Top 16	20268	1125	389	0	0	0	0
Top 17	10319	0	1104	381	0	0	0
Top 18	28854	897	528	17	0	0	0
Top 19	19839	0	199	0	1	0	1058
Top 20	29870	237	776	36	9	55	113
Top 21	36	32	694	22	117	192	105
Top 22	29784	4	157	0	0	1	794
Top 23	15933	0	153	0	0	0	705
Top 24	11083	142	590	32	12	21	55
Top 25	11916	1	822	9	0	0	12

Table 14: Cluster statistics for states with more than 50 SARS-CoV-2 genome samples.

State	Cluster A	Cluster B	Cluster C	Cluster D	Cluster E	Cluster F
New Hampshire	330	1743	25	442	870	1082
New York	1461	918	108	2	210	451
Kansas	425	1461	302	0	3	332
Wisconsin	328	1189	20	0	12	192
Missouri	944	592	16	2	28	73
North Dakota	310	701	183	0	121	41
Alaska	55	505	319	0	1	7
Arizona	442	267	28	1	16	104
South Dakota	260	385	56	0	14	140
Utah	266	236	100	0	46	30
District of Columbia	232	222	7	5	15	53
Hawaii	79	148	3	0	1	16
Kentucky	91	89	36	0	2	11
Maine	59	85	0	11	4	17
Delaware	44	87	10	0	17	10
Wyoming	12	47	5	11	41	41
Arkansas	24	49	22	0	0	46
Oregon	41	69	6	0	10	12
South Carolina	10	33	71	4	7	0
Texas	35	71	0	1	12	2
Tennessee	45	27	26	1	14	7
Washington	18	72	4	1	5	6
Minnesota	69	17	0	0	7	4
New Mexico	40	28	10	0	0	11
Mississippi	53	28	0	0	1	1
Vermont	22	42	0	1	8	3
Indiana	6	62	1	0	0	0
New Jersey	27	5	5	0	5	9
California	21	14	0	0	0	15

Table 15: The world wide clusters from SARS-CoV-2 genome data available up to June 01, 2020. The listed countries are the United States (US), Canada (CA), Australia (AU), United Kingdom (UK), Germany (DE), France (FR), Italy (IT), Russia (RU), China (CN), Japan (JP), Korean (KR), India (IN), Spain (ES), Saudi Arabia (SA), and Turkey (TR). [31].

Country	Cluster I	Cluster II	Cluster III	Cluster IV	Cluster V	Cluster VI
US	844	311	488	156	1813	975
CA	12	29	17	16	19	41
AU	163	149	410	135	146	77
UK	539	875	908	1532	119	3
DE	10	20	21	38	42	0
FR	41	85	14	12	82	0
IT	26	24	9	17	0	0
RU	10	27	1	109	3	0
CN	8	3	215	1	1	25
JP	0	3	68	20	3	0
KR	0	0	28	0	0	0
IN	93	69	141	10	3	0
ES	27	100	74	25	3	2
SA	14	31	9	1	2	0
TR	25	3	24	9	0	0

Table 16: The world wide clusters from SARS-CoV-2 genome data available up to June 01, 2020 using PCA embedding with reduction ratio of 1/160.

Country	Cluster I _p	Cluster II _p	Cluster III _p	Cluster IV _p	Cluster V _p	Cluster VI _p
US	915	489	239	156	1813	975
CA	14	17	27	16	19	41
AU	164	414	143	136	146	77
UK	543	908	857	1546	119	3
DE	10	21	20	38	42	0
FR	46	14	80	12	82	0
IT	26	9	24	17	0	0
RU	10	1	27	109	3	0
CN	8	213	3	1	1	24
JP	0	68	3	20	3	0
KR	0	28	0	0	0	0
IN	95	141	67	10	3	0
ES	27	74	100	25	3	2
SA	30	9	15	1	2	0
TR	27	24	1	9	0	0

Table 17: The world wide clusters from SARS-CoV-2 genome data available up to June 01, 2020 using UMAP embedding with reduction ratio of 1/160

Country	Cluster I _u	Cluster II _u	Cluster III _u	Cluster IV _u	Cluster V _u	Cluster VI _u
US	2446	1096	90	751	110	94
CA	71	15	9	35	1	3
AU	784	94	64	18	83	37
UK	2171	115	828	2	534	326
DE	57	40	14	0	5	15
FR	163	45	10	0	11	5
IT	13	1	35	0	5	22
RU	92	2	49	0	0	7
CN	178	28	6	10	22	6
JP	36	0	11	0	47	0
KR	18	0	0	1	9	0
IN	232	3	7	0	2	72
ES	205	2	12	0	7	5
SA	56	0	1	0	0	0
TR	56	1	4	0	0	0